

Near-Field Optical Drilling of Sub- λ Pits in Thin Polymer Films

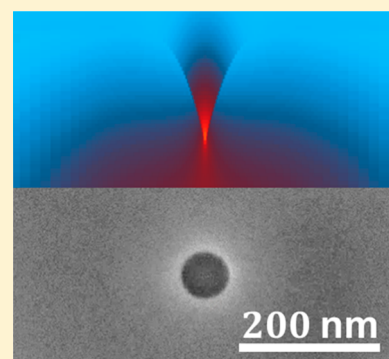
Tao Ding,* Rohit Chikkaraddy, Jan Mertens, and Jeremy J. Baumberg*

Nanophotonics Centre, Cavendish Laboratory, University of Cambridge, Cambridge, CB3 0HE, United Kingdom

Supporting Information

ABSTRACT: Under UV illumination, polymer films can undergo chain scission and contract. Using this effect, tightly focused laser light is shown to develop runaway near-field concentration that drills sub-100 nm pits through a thin film. This subwavelength photolithography can be controlled in real time by monitoring laser scatter from the evolving holes, allowing systematic control of the void diameter. Our model shows how interference between the substrate and film together with near-field focusing by the evolving crevice directs this formation and predicts minimum pit sizes in films of 100 nm thickness on gold substrates. The smallest features so far are 60 nm diameter pits using 447 nm light focused onto polystyrene through a $\times 100$ objective ($NA = 0.8$). Such arrays of pits can be easily used as masks for fabricating more complex nanostructures, such as plasmonic nanostructures and biomicrofluidic devices. This demonstration shows the potential for harnessing near-field feedback in optical direct-writing for nanofabrication.

KEYWORDS: photolithography, diffraction limit, photodegradation, polystyrene, crevices



Nanolithography technologies play a significant role in the fabrication of nanodevices for integrated electronic circuits, optics, and biochips.¹ Traditional lithography techniques such as photolithography,² soft lithography,³ beam pen lithography,⁴ and imprint lithography⁵ need expensive mask/master preparation, which have to be replaced every time the pattern is changed. Electron-beam lithography, although achieving high resolutions (<10 nm) for arbitrary patterns, is very expensive and operates in vacuum.⁶ Optical direct-write techniques (either single-photon or two-photon) use dedicated photoresists, however, their resolution is still diffraction limited in most cases, even with advanced surface transfer techniques.⁷ While this limitation can be scaled by using extreme-ultraviolet wavelengths,⁸ this again requires vacuum processing.⁹ Photo-thermal effects can yield holes in polymer films, but only larger than 100 nm.^{10–13} Recent developments of stimulated emission depletion microscopy in combination with two-photon lithography have yielded feature sizes of 120 nm^{14–16} or even smaller,^{17,18} but specialized photoresists, photoinitiators, and photoinhibitors are required together with an additional inhibition laser beam, adding cost and complexity.

Here, spontaneous near-field light concentration is found to produce sub-100 nm pits in polystyrene (PS) films. The intense optical field concentrated in the developing crevice accelerates the photodegradation of the polymer film coated on gold. The size of the pits can be tuned below the diffraction limit, controllably from 60 nm to 1 μm by monitoring light scattering from the pits. This strongly contrasts with other near-field lithography techniques such as contact imaging, which use the near-field to transfer an already subwavelength pattern (produced by EUV or electron beam fabrication) into deeper layers.¹⁹ Although scanning near-field optical lithography can write subdiffraction patterns, it suffers from slow scan speeds

due to the need to move a mechanical near-field probe across the sample maintaining subwavelength proximity.²⁰

The optical drilling process starts with 100 nm PS films which are spin-coated onto Au substrates (Figure 1). A laser with wavelength of 447 nm is focused down onto the surface of the film through a $\times 100$ dark field objective with $NA = 0.8$ (Figure 1b, inset, see Supporting Information (SI) Scheme S1 for details). The white-light scattering peak gradually increases and red-shifts as the irradiation proceeds, which indicates the growth of a pit (Figure 1a). The increasing scattering intensity extracted at 560 nm (red line, Figure 1b) shows the evolving increase in pit size, allowing us to monitor the growth in real time. We define the effective diameter of the pits using the full-wave-half-maximum (fwhm) of the depth profile. The rapid degradation process via free radicals causes the pit to widen and deepen into a hole of size >200 nm in less than a second (SI, Figure S1). More sensitive feedback is provided by the scattered laser light (blue line, Figure 1b), which shows a sharp increase at the beginning of pit formation. This allows irradiation to be terminated within 100 ms of the pit initiating. We use a threshold scattering rate, S_{th} , to shut off the laser, with S measured as the rate of increase in laser scattering (Figure 1b). Irradiating an array (pitch 1 μm) in PS films using $S_{\text{th}} = 2$ forms pits of 65 ± 5 nm in fwhm (Figure 1c,e), far below the diffraction limit (175 nm) of the laser (447 nm, $NA = 0.8$). Evaporating a 30 nm Au layer on top of the PS film shrinks the size of the pits to 45 ± 5 nm (Figure 1d). The AFM profiles show pit depths of 45 ± 5 nm with good consistency (Figure 1e), but the AFM measurements do not reflect the full pit depth due to the AFM probe width. By controlling S_{th} , pits with

Received: December 15, 2016

Published: May 25, 2017

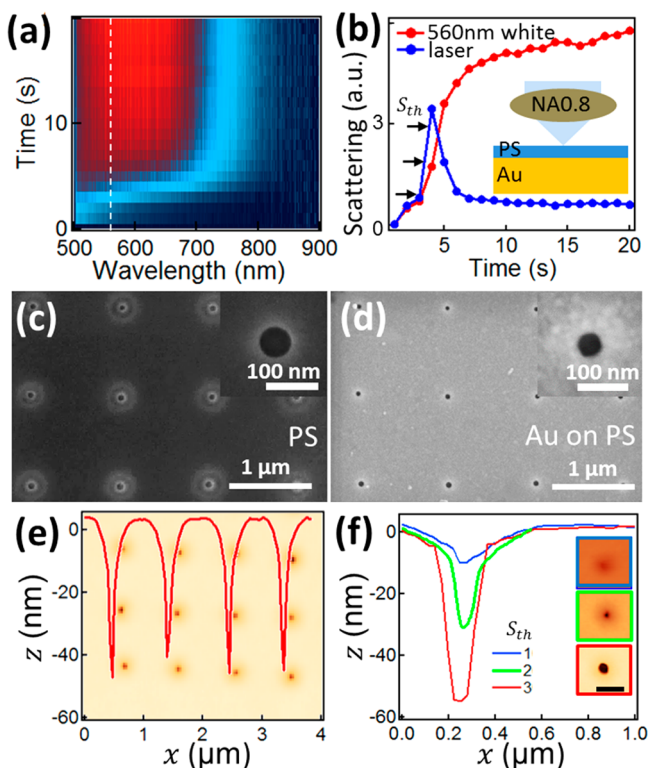


Figure 1. Fabricating sub-100 nm pits by monitoring the scattering kinetics. (a) Scattering kinetics during laser irradiation (447 nm, 3 mW). (b) Scattering intensity vs time of UV laser and white light at 560 nm. (c) SEM image of laser-drilled pits with (d) evaporated Au (30 nm) on top. (e) AFM profiles of pits in (c). (f) Pits drilled with different scattering thresholds (S_{th}), with inset AFM images. Scale bar is 500 nm.

different sizes and depths are obtained (Figure 1f), showing how the pit grows with light dosage. Initially, a shallow depression with a diameter matching the focused laser beam forms, followed by rapid deepening and narrowing into a cone shape (Figure 1f and SI, Figure S2). Further growth gives wider and deeper holes. Clearly, some new mechanism beyond

geometric optics has to be involved in the sharp narrowing of the pit size, because diffraction places absolute limits on the focal spot size.

This polymer photodegradation process cannot be due to photothermal effects as estimates of the local temperature increase caused by irradiating the metallic film are less than 10 °C for the powers applied (4–10 mW/ μm^2).²¹ Moreover, such optical drilling does not work on PMMA films unless much higher powers (>12 mW/ μm^2) are applied for longer irradiation times (30 s), and even then the pits produced are much shallower (SI, Figure S3). This evidence of chemical selectivity suggests that the degradation of PS is likely to be a photochemical process,^{22,23} in which free radicals break vinyl bonds and benzyl rings in the presence of oxygen at the surface.²⁴ Further evidence suggesting subsequent photochemical changes is that irradiated regions of PS film close to the substrate cannot be dissolved in toluene, leaving arrays of thin polymer pads (35 nm in height) on the gold (SI, Figure S4). Cross-linking must occur near the substrate surface where no oxygen is present.

Although PS has strongest absorbance around 240 nm in the UV, it quickly develops induced absorbance at wavelengths up to 490 nm after initial chain scission, which makes photodegradation with a 447 nm CW laser possible.²⁵ One possibility is that this initial trigger occurs via multiphoton ablation,²⁶ which has been shown to occur in polymers even from CW lasers.^{26,27} Using the two-photon cross section of benzene at 455 nm²⁸ (which sets the polystyrene response) indeed suggests that it dominates over the one photon absorption tail and implies that the initial stage is triggered by two-photon absorption, which rapidly enhances the one-photon absorption that subsequently drives hole drilling. Direct confirmation is, however, complicated by the nonlinear evolution discussed further below. We highlight that improved understanding of optically driven ablation mechanisms in polystyrene and other polymers is thus of considerable interest for such lithography.

To explore how focused illumination and photochemical degradation can result in sub-100 nm pits, we vary the PS film thickness t (Figure 2a–c) and substrate material (Figure 2d–f). We find that as the film gets thicker, irradiation for the same S_{th}

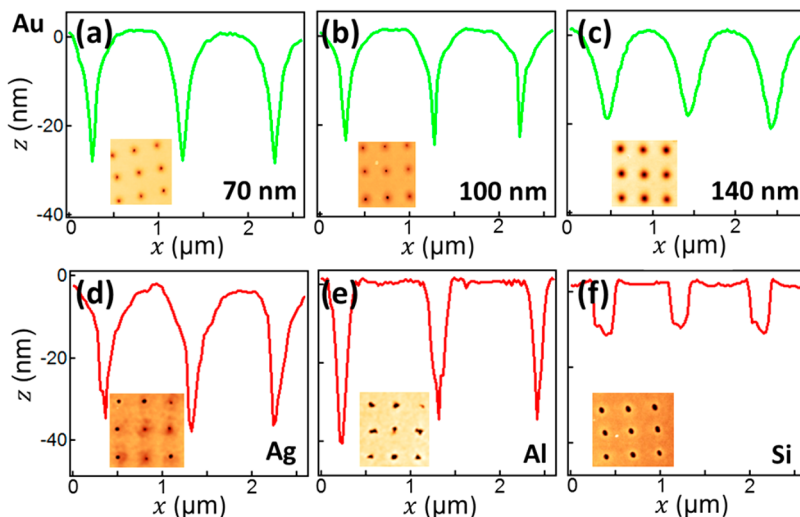


Figure 2. AFM profiles of pits in PS formed under different conditions. (a–c) Dependence on PS film thickness (on Au at $S_{th} = 2$): (a) 70, (b) 100, and (c) 140 nm. (d–f) Substrate dependence of pits formed at $S_{th} = 3$ on (d) Ag, (e) Al, and (f) Si; PS film thickness is 100 nm. Insets are corresponding AFM images.

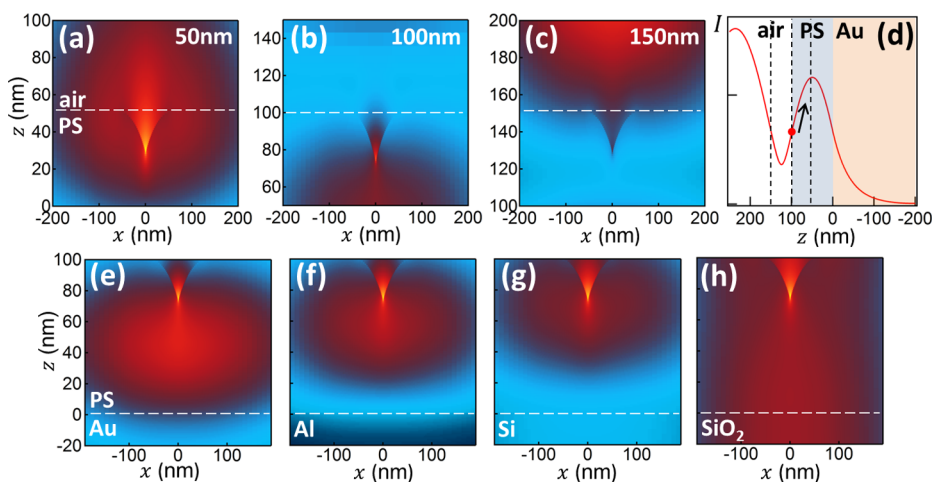


Figure 3. FDTD simulations of near field distributions. (a–c) PS films of different thickness on Au (as marked). (d) Intensity of 447 nm light above planar PS/Au films, with dashed lines showing the three film thicknesses. (e–h) Substrate dependence of 100 nm PS films on different substrates: (e) Au, (f) Al, (g) Si, and (h) SiO₂. Light distributions are normalized, while artificial pit is imposed initially.

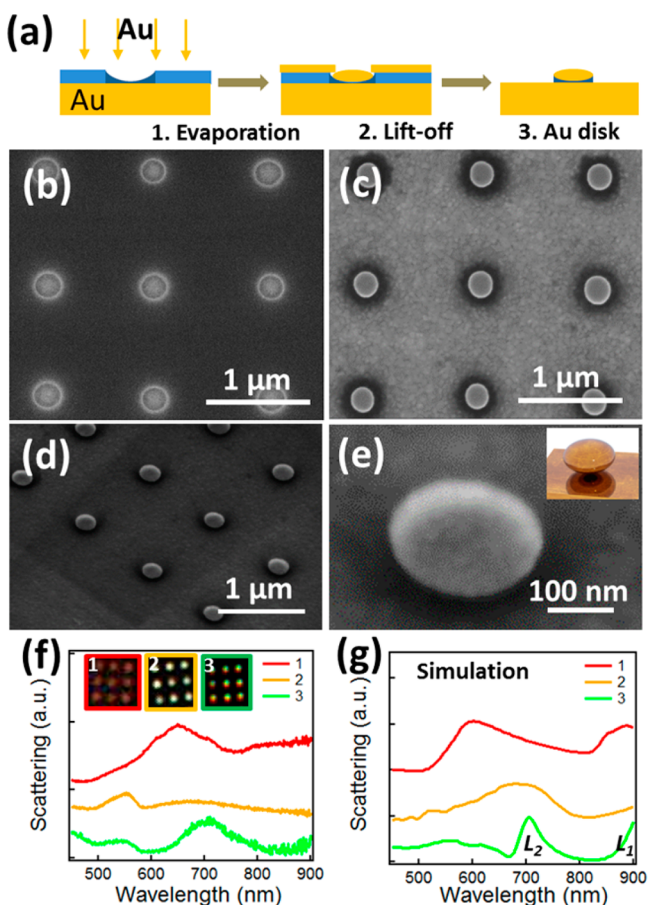


Figure 4. Fabrication of Au nanoparticle arrays. (a) Fabrication scheme. (b–e) SEM images of (b) hole array (used as mask) and Au NPOM arrays from (c) top view, (d) tilted 45° view, and (e) magnified view. Inset is oblate spheroidal Au NPOM. (f) Scattering spectra of fabricated structures from (a): (1) optical drilled holes, (2) with Au evaporated on top, and (3) after lift-off. Insets show corresponding dark field optical images. (g) Simulation of scattering from nanostructures at process stages as in (f).

results in shallower pits, with sharpest pits for film thicknesses of $t = 100$ nm. The scattering kinetics of these films presents

different spectral features mainly due to interference of the scattered light for different film thickness (SI, Figure S5). However, they all show a similar depth profile, with the depth developing from a 400 nm wide surface depression, quickly narrowing down with depth (sharpest for $t = 100$ nm). The substrate also influences pit formation significantly (Figure 2d,e), with Ag and Al most similar, though less reproducible than Au. Pits formed on Si substrates are much shallower and wider (Figure 2f), while no pits can be formed on glass substrates. Scattering kinetics reveals that pits form first on Ag, then Al and Au, and finally Si, under the same irradiation power (SI, Figure S6).

These results suggest that thin film optics plays a crucial role in the drilling kinetics of the PS. The near-field distributions from 3D finite difference time domain (FDTD) simulations show that light is more confined within the crevices for PS thicknesses of 100 nm (Figure 3a–c). This is due to two effects. The first is the constructive interference of light above the reflective substrate which locates a standing wave maximum below the top of the PS only for $t = 100$ nm. The second effect is the concentration of light in the developing crevice, due to constructive interference from reflections off each side. For $t = 100$ nm, when a dip forms in the PS surface, the bottom of the dip experiences a higher intensity and thus faster photochemical degradation. This narrows and deepens the pit, further increasing the intensity at the bottom and its etching rate. As a result, near-field drilling will only occur where the intensity increases as the pit deepens (Figure 3d, red point), matching the experimental results (Figure 2b).

The dependence on substrate material can also be understood from this model. While Al and Si are highly reflective at 447 nm producing standing waves more than 60 nm above the metal surface (Figure 3f,g), Au has interband transitions at this wavelength and its standing wave is phase shifted closer (Figure 3e). This means that the evolving pit above Al or Si rapidly reaches a depth where the light decreases with further etching, thus blunting the runaway process resulting in wider and shallower pits. For Au substrates the increasing pit etching rate persists nearly down to the substrate, while for glass substrates (Figure 3h) there is no reflection to give standing waves and the laser intensity is below the photochemical threshold. Although the field profile above a Ag substrate is similar to the

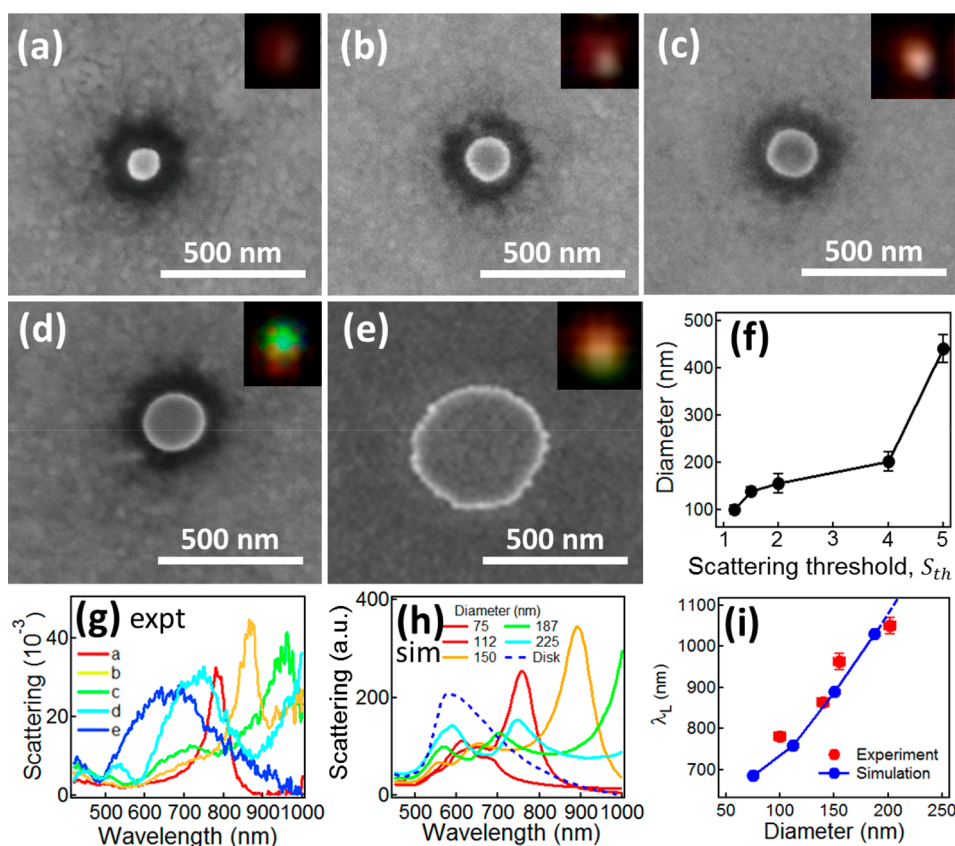


Figure 5. Au NPoMs of increasing size. (a–e) SEM images of Au NPoMs of different sizes. Insets are dark field images. (f) Change of Au NPoM sizes with scattering threshold value. (g) Experimental and (h) simulation of scattering spectra of Au NPoMs with different sizes. (i) Shift of coupled plasmon resonances (dipolar mode) with increasing size of the Au NPoM. The longest-wavelength dipolar mode (cyan curve) shifts out of the detection range, and its value is therefore estimated.

Au substrate (Figure S7), its relative poor reproducibility in creating nanoholes may arise from surface oxidation, which changes the actual field distribution. The sub-100 nm pits are thus formed due to near field concentration feedback effects caused by interference in three dimensions.

From this understanding and controllability of the optical near-field drilling process, we can make arrays of holes with sizes ranging from 60 nm to 1 μm and use them as deposition or etch masks for the fabrication of more complicated plasmonic nanostructures, such as arrays of holes in Au films (SI, Figure S8) or Au nanoparticle-on-mirror (NPoM) arrays (Figure 4). For strong plasmonic coupling and easy characterization, we fabricate 215 ± 15 nm holes (Figure 4b) and then evaporate 40 nm Au on top, followed by lift-off in toluene (Figure 4a). The resulting Au pattern shows good reproducibility and uniformity of the particles, with a diameter of 225 ± 10 nm (Figure 4c,d). The magnified view shows their oblate spheroidal shape arising from the shape of the holes (Figure 4e). Characterization by AFM shows that the Au nanoparticle is 70 nm high, suggesting there is a 30 nm polymer pad underneath the 40 nm Au, which matches previous results (SI, Figure S4). The scattering spectra from these arrays (Figure 4f) directly track the change of nanostructures from PS holes to Au NPoMs, and agree well with simulations (Figure 4g). The spectra are sensitive to all the nanostructure dimensions (details will be discussed elsewhere) and serve to show how plasmonic coupled structures can be easily produced by this simple near-field direct-write photolithography.

As the size of the pits can be controlled through S_{th} , which stops laser irradiation before larger holes evolve (Figure 1f), a series of Au NPoMs with increasing size can be produced (Figure 5a–f). The scattering spectra show a gradual red shift of the coupled modes for larger sizes (Figure 5h), which matches simulation results very well (Figure 5i). When the diameter of the Au NP exceeds 400 nm, its shape changes from spheroid to disk (Figure 5e), which changes the scattering spectra completely and no longer follows the trend of redshifts (blue lines in Figure 5g,h). This shows the flexibility of the nanofabrication possible using this technique, with a wide variety of pit/hole and particle shapes and spacings. Note that attempts to drill nanopits in close proximity are complicated by additional near-field scattering from the existing pit, though it is possible with larger holes (SI, Figure S9). Using alternative (such as elliptical) shaped focal spots should also modify the pit circularity. The mechanism introduced here may also be implicated in the recent demonstration of two-photon lithography of resists which produces microexplosions at >10 mW 532 nm power CW irradiation.²⁷ Full understanding of the interaction of light with polymer films including local bond breaking and cross-linking is crucial for advanced direct-write lithographies but involves near-field interactions.

We also note here other nonlinear processes that have been seen to access subwavelength features. Conventional far-field two-/multiphoton lithographies rarely give features smaller than 200 nm^{29–34} unless STED-derived techniques are incorporated (which are costly to implement).^{16,17} Alternative plasmon-enhanced multiphoton processes^{35–37} (which are

more complex to exploit) differ from the near-field enhanced mechanism here, which arises from the nonlinear resculpting of the local film deformation.

In conclusion, we have developed a near-field-enhanced photolithography based on the photochemistry of thin polymer films. The synergistic effects of 100 nm thick PS films and Au substrates produces constructive interference in the evolving crevice, thereby generating strongly localized optical fields which constrain photodegradation of PS to regions far smaller than the diffraction limit of light. Real-time spectroscopic monitoring of the pit drilling process enables smallest pit sizes currently of 60 nm. This can be further improved using lasers of shorter wavelength and objectives with higher NA, but should be possible to extend to a wide range of polymeric films and substrates. This technique brings new opportunities for sub-100 nm structuring based on near-field direct-write lithography (NF-DWL) at low cost. This high resolution DWL can place nanostructures accurately, and enables rapid prototyping of advanced electronics and photonics devices.

■ ASSOCIATED CONTENT

● Supporting Information

The Supporting Information is available free of charge on the ACS Publications website at DOI: 10.1021/acsphotonics.6b01000.

Experimental details, SEM images of irradiation time series, irradiation of PMMA films, fabrication of PS pad arrays, thickness and substrate dependence on the scattering kinetics, fabrication of Au hole arrays, SEM images of holes with different separations, and FDTD simulation model setup and result for Ag substrate (PDF).

■ AUTHOR INFORMATION

Corresponding Authors

*E-mail: t.ding@whu.edu.cn.

*E-mail: jjb12@cam.ac.uk.

ORCID

Jeremy J. Baumberg: 0000-0002-9606-9488

Author Contributions

T.D. conceived the idea and performed the experiments. J.M. built the setup and wrote the codes for irradiation control. R.C. did the FDTD simulations. T.D. and J.J.B. analyzed the data, built the model, and wrote the manuscript. All authors have given approval to the final version of the manuscript.

Funding

EPSRC Grant: EP/G060649/1, EP/N016920/1, and EP/L027151/1; ERC Grant: LINASS 320503; Leverhulme Trust: ECF-2016-606.

Notes

The authors declare no competing financial interest. Raw data of the figures shown in this paper can be found at <https://doi.org/10.17863/CAM.9981>.

■ ACKNOWLEDGMENTS

This research is supported by UK Engineering and Physical Sciences Research Council Grants EP/G060649/1, EP/N016920/1, and EP/L027151/1, ERC Grant LINASS 320503, and Leverhulme Trust (ECF-2016-606). R.C. acknowledges support from the Dr. Manmohan Singh scholarship from St John's College, University of Cambridge.

■ REFERENCES

- (1) Feldman, M. *Nanolithography*, 1st ed.; Woodhead Publishing: Cambridge, 2014; pp 348–441.
- (2) Berkowski, K. L.; Plunkett, K. N.; Yu, Q.; Moore, J. S. Introduction to Photolithography: Preparation of Microscale Polymer Silhouettes. *J. Chem. Educ.* **2005**, *82*, 1365.
- (3) Qin, D.; Xia, Y.; Whitesides, G. M. Soft Lithography for Micro- and Nanoscale Patterning. *Nat. Protoc.* **2010**, *5*, 491–502.
- (4) Huo, F.; Zheng, G.; Liao, X.; Giam, L. R.; Chai, J.; Chen, X.; Shim, W.; Mirkin, C. A. Beam Pen Lithography. *Nat. Nanotechnol.* **2010**, *5*, 637–640.
- (5) Schiff, H. Nanoimprint Lithography: An Old Story in Modern Times? A Review. *J. Vac. Sci. Technol. B* **2008**, *26*, 458–480.
- (6) Chen, Y. Nanofabrication by Electron Beam Lithography and Its Applications: A Review. *Microelectron. Eng.* **2015**, *135*, 57–72.
- (7) Osgood, R. M.; Gilgen, H. H. Laser Direct Writing of Materials. *Annu. Rev. Mater. Sci.* **1985**, *15*, 549–576.
- (8) Henderson, C.; Wheeler, D.; Pollagi, T.; Cardinale, G.; O'Connell, D.; Fisher, A.; Rao, V.; Goldsmith, J. Top Surface Imaging for Extreme Ultraviolet Lithography. *J. Photopolym. Sci. Technol.* **1998**, *11*, 459–464.
- (9) Wu, B.; Kumar, A. Extreme Ultraviolet Lithography: A Review. *J. Vac. Sci. Technol. B* **2007**, *25*, 1743–1761.
- (10) Singer, J. P.; Lin, P.-T.; Kooi, S. E.; Kimerling, L. C.; Michel, J.; Thomas, E. L. Direct-Write Thermocapillary Dewetting of Polymer Thin Films by a Laser-Induced Thermal Gradient. *Adv. Mater.* **2013**, *25*, 6100–6105.
- (11) Kappes, R. S.; Schönfeld, F.; Li, C.; Golriz, A. A.; Nagel, M.; Lippert, T.; Butt, H.-J.; Gutmann, J. S. A Study of Photothermal Laser Ablation of Various Polymers on Microsecond Time Scales. *SpringerPlus* **2014**, *3*, 1–15.
- (12) Wei, J.; Wang, R. Maskless Direct Laser Writing with Visible Light: Breaking through the Optical Resolving Limit with Cooperative Manipulations of Nonlinear Reverse Saturation Absorption and Thermal Diffusion. *J. Appl. Phys.* **2014**, *115*, 123102.
- (13) Avrutsky, I.; Georgiev, D. G.; Frankstein, D.; Auner, G.; Newaz, G. Super-Resolution in Laser Annealing and Ablation. *Appl. Phys. Lett.* **2004**, *84*, 2391–2393.
- (14) Fischer, J.; Wegener, M. Three-Dimensional Optical Laser Lithography Beyond the Diffraction Limit. *Laser Photon. Rev.* **2013**, *7*, 22–44.
- (15) Fischer, J.; Wegener, M. Three-Dimensional Direct Laser Writing Inspired by Stimulated-Emission-Depletion Microscopy. *Opt. Mater. Express* **2011**, *1*, 614–624.
- (16) Wollhofen, R.; Katzmann, J.; Hrelescu, C.; Jacak, J.; Klar, T. A. 120 nm Resolution and 55 nm Structure Size in Sted-Lithography. *Opt. Express* **2013**, *21*, 10831–10840.
- (17) Gan, Z.; Cao, Y.; Evans, R. A.; Gu, M. Three-Dimensional Deep Sub-Diffraction Optical Beam Lithography with 9 nm Feature Size. *Nat. Commun.* **2013**, *4*, 2061.
- (18) Cao, Y.; Gan, Z.; Jia, B.; Evans, R. A.; Gu, M. High-Photosensitive Resin for Super-Resolution Direct-Laser-Writing Based on Photoinhibited Polymerization. *Opt. Express* **2011**, *19*, 19486–19494.
- (19) Fischer, U. C.; Zingsheim, H. P. Submicroscopic Pattern Replication with Visible Light. *J. Vac. Sci. Technol.* **1981**, *19*, 881–885.
- (20) Credgington, D.; Fenwick, O.; Charas, A.; Morgado, J.; Suhling, K.; Cacialli, F. High-Resolution Scanning near-Field Optical Lithography of Conjugated Polymers. *Adv. Funct. Mater.* **2010**, *20*, 2842–2847.
- (21) Emmerich, R.; Bauer, S.; Ploss, B. Temperature Distribution in a Film Heated with a Laser Spot: Theory and Measurement. *Appl. Phys. A: Solids Surf.* **1992**, *54*, 334–339.
- (22) Turzyński, Z.; Witkowski, K.; Woliński, L.; Szafko, J. Simultaneous Scission and Crosslinking of Polystyrene Chains on Irradiation by Ultraviolet Light in CCl₄ and CHCl₃ Solutions. *J. Polym. Sci., Part B: Polym. Phys.* **1990**, *28*, 467–479.
- (23) Zhang, D.; Dougal, S. M.; Yeganeh, M. S. Effects of UV Irradiation and Plasma Treatment on a Polystyrene Surface Studied by

IR–Visible Sum Frequency Generation Spectroscopy. *Langmuir* **2000**, *16*, 4528–4532.

(24) Yousif, E.; Haddad, R. Photodegradation and Photostabilization of Polymers, Especially Polystyrene: Review. *SpringerPlus* **2013**, *2*, 1–32.

(25) Nurmukhametov, R. N.; Volkova, L. V.; Kabanov, S. P. Fluorescence and Absorption of Polystyrene Exposed to UV Laser Radiation. *J. Appl. Spectrosc.* **2006**, *73*, 55–60.

(26) Xiong, W.; Zhou, Y. S.; He, X. N.; Gao, Y.; Mahjour-Samani, M.; Jiang, L.; Baldacchini, T.; Lu, Y. F. Simultaneous Additive and Subtractive Three-Dimensional Nanofabrication Using Integrated Two-Photon Polymerization and Multiphoton Ablation. *Light: Sci. Appl.* **2012**, *1*, e6.

(27) Thiel, M.; Fischer, J.; Freymann, G. v.; Wegener, M. Direct Laser Writing of Three-Dimensional Submicron Structures Using a Continuous-Wave Laser at 532 nm. *Appl. Phys. Lett.* **2010**, *97*, 221102.

(28) Tam, A. C.; Patel, C. K. N. Two-Photon Absorption Spectra and Cross-Section Measurements in Liquids. *Nature* **1979**, *280*, 304–306.

(29) Ovsianikov, A.; Chichkov, B. N. Two-Photon Polymerization – High Resolution 3d Laser Technology and Its Applications. In *Nanoelectronics and Photonics: From Atoms to Materials, Devices, and Architectures*; Korin, A., Rosei, F., Eds.; Springer New York: New York, NY, 2008; pp 427–446.

(30) Zhou, X.; Hou, Y.; Lin, J. A Review on the Processing Accuracy of Two-Photon Polymerization. *AIP Adv.* **2015**, *5*, 030701.

(31) Maria, F.; Maria, V.; Boris, N. C. Multiphoton Polymerization of Hybrid Materials. *J. Opt.* **2010**, *12*, 124001.

(32) Wang, I.; Bouriau, M.; Baldeck, P. L.; Martineau, C.; Andraud, C. Three-Dimensional Microfabrication by Two-Photon-Initiated Polymerization with a Low-Cost Microlaser. *Opt. Lett.* **2002**, *27*, 1348–1350.

(33) Baldacchini, T.; Snider, S.; Zadoyan, R. Two-Photon Polymerization with Variable Repetition Rate Bursts of Femtosecond Laser Pulses. *Opt. Express* **2012**, *20*, 29890–29899.

(34) Malinauskas, M.; Danilevičius, P.; Juodkazis, S. Three-Dimensional Micro-/Nano-Structuring Via Direct Write Polymerization with Picosecond Laser Pulses. *Opt. Express* **2011**, *19*, 5602–5610.

(35) Cohanoschi, I.; Yao, S.; Belfield, K. D.; Hernández, F. E. Effect of the Concentration of Organic Dyes on Their Surface Plasmon Enhanced Two-Photon Absorption Cross Section Using Activated Au Nanoparticles. *J. Appl. Phys.* **2007**, *101*, 086112–086112–3.

(36) Lim, C. K.; Li, X.; Li, Y.; Drew, K. L.; Palafoxhernandez, J. P.; Tang, Z.; Baev, A.; Kuzmin, A. N.; Knecht, M. R.; Walsh, T. R. Plasmon-Enhanced Two-Photon-Induced Isomerization for Highly-Localized Light-Based Actuation of Inorganic/Organic Interfaces. *Nanoscale* **2016**, *8*, 4194–4202.

(37) Zhang, T.; Zhao, T.; Yuan, P.; Xu, Q.-H. Plasmon-Enhanced Two-Photon Excitation Fluorescence and Biomedical Applications. In *Surface Plasmon Enhanced, Coupled and Controlled Fluorescence*; John Wiley & Sons, Inc., 2017; pp 211–225.